Supporting Information for "Tracer variability and stirring in the Antarctic Circumpolar Current"

Dhruv Balwada[1], Alison R. Gray[2], Lilian A. Dove[3], and Andrew F. Thompson[3]

[1]Lamont-Doherty Earth Observatory, Columbia University, Palisades, NY, USA

[2]School of Oceanography, University of Washington, Seattle, WA, USA

[3]Division of Geological and Planetary Sciences, Environmental Science and Engineering, California Institute of Technology, Pasadena, CA, USA

1. Supplemental details for Data and Methods

1.1. Glider data processing

The glider data was first processed using the Seaglider toolbox. The Seaglider toolbox performs a number of quality control and calibration tasks, which include removing extreme spikes in salinity, correcting for thermal lag, etc. (A summary of these automatic QC steps is given in: `https://gliderfs2.coas.oregonstate.edu/sgliderweb/Seaglider_Quality_Control_Manual.html`). The primary variables, often referred to as data in this section, considered in this study are the temperature, salinity, and oxygen measurements collected by the gliders. A few extra calibration procedures were applied to the data to correct for sensor biases, which primarily involved doing additive corrections to the processed measurements to ensure that the gliders and the Argo floats had similar distribution medians (details of the exact additive values can be found in Dove, Thompson, Balwada, and Gray (2021)).

In addition, we performed a few more quality control and smoothing operations to get the data into a form that was appropriate to use for understanding the small scale properties. Specifically, we despiked the data using a 12 point median filter, where the filter width was chosen such that the standard deviation of the spike anomalies did not change drastically on increasing the window size further. Then we re-sorted the data from each profile to ensure that there were no density overturns, which is acceptable since we are primarily interested in ocean dynamics that don't create overturns. Finally, we vertically bin averaged the data into 4m bins to provide a small degree of additional smoothing. This gridded dataset was also mapped onto isopycnals using linear interpolation for some of the analysis, where the isopycnals were defined using potential density referenced to the surface and the vertical grid size in isopycnal space was chosen to be 0.001 kg m^{-3}.

In sections where a uniform gridding in the horizontal direction was required, such as when computing the spectra, we did a linear interpolation onto a fine horizontal grid. This interpolation was done onto a 500 m grid when considering properties in the along-track distance, and 1 hour when considering properties in time; both grid sizes chosen to be smaller than most of sampling resolution (Figure S1). This linear interpolation procedure does not introduce any additional structure in the data, and the spectra at the scales smaller than the observed scales are highly muted - variance drops rapidly when there are not many samples at those scale (see appendix of Klymak, Crawford, Alford, MacKinnon, and Pinkel (2015)).

1.2. Spice

Spice (τ) is a variable that is used to quantify the thermohaline variations along isopycnals (Stommel, 1962; McDougall & Krzysik, 2015), and is defined in differential form as,

$$d\tau = \rho_0(\alpha dT + \beta dS) = 2\alpha dT = 2\beta dS. \quad (1)$$

where α and β are the thermal and haline expansion coefficients. The second and third equality result from the fact that along an isopycnal $\alpha dT = \beta dS$. Here the anomalies, such as dT, are defined relative to the along isopycnal mean T-S profile averaged over all the profiles collected by the glider. For our analysis using the spice anomaly ($d\tau$) is sufficient and we do not need to estimate the integral or absolute value, as we only analyze the spice variations along isopycnals. Defining an absolute value of spice is not very useful, as it is not a variable that can be quantitatively compared across isopycnals. But qualitative patterns like locally vertically coherent anomalies in the spice anomaly can be used to identify watermasses that might have similar origins and history. For our dataset, using spice is comparable to using temperature, since the density variations are dominated by salinity gradients and temperature gradients play a minor role in setting the density field and instead are stirred as passive anomalies.

1.3. Data processing to compute the diapycnal spice curvature

The diapycnal spice curvature (DSC) is defined as,

$$\tau_{\rho\rho} = \frac{1}{\rho_z}\left(\frac{\alpha T_z + \beta S_z}{-\alpha T_z + \beta S_z}\right) \approx 2\alpha\rho T_{\rho\rho} \approx 2\beta\rho S_{\rho\rho} \tag{2}$$

and is a good visual indicator of water mass interleaving. Since the DSC is the second derivative, it is a noisy quantity and requires some smoothing before it can be computed.

Here we smoothed the spice along the density axis using a n-point running mean filter applied twice before computing the cross-isopycnal gradients. The isopycnal grid had a resolution of 0.001 kg m^{-3}. The sensitivity to the choice of 'n' is shown in Figure S2. A visual comparison of the different filter scales shows that the overall qualitative patterns are not sensitive to the choice of the filter scale, and all the filter scale choice result in similar conclusions. The layering plots in the main text were plotted with $n = 30$.

1.4. Details of the multi-taper method for spectral estimation

We use the multi-taper (MT) method to perform the spectral estimation, which can be understood using the practical summary of the spectral estimation and MT method presented in Prerau, Brown, Bianchi, Ellenbogen, and Purdon (2017). Here we used the python package Spectrum to do the estimation (Cokelaer & Hasch, 2017). The MT method uses a number of orthogonal taper windows to generate multiple independent estimates of the spectrum from the dataset, in contrast to a single taper window that is routinely used in oceanography. These independent estimates are then averaged to generate a more reliable estimate, where accuracy is improved at the cost of reduced range of wavenumbers over which the spectra is estimated. These MT estimates are calculated independently for each of the two gliders and then averaged together to provide the final estimate presented in the results.

An important parameter that needs to be selected in the MT method is the time-half-bandwidth parameter, N_w, where a larger value results in a smoother estimate (Prerau et al., 2017). However, a larger value also results in the low-frequency plateau, often seen in log-log plots of oceanographic spectra, to extend to larger frequencies and potentially steepen the power-law dependence that is often observed, as a larger value is resulting is more smoothing. Here we choose N_w to be 10 hours when estimating the frequency spectrum and 2.5 km when estimating the wavenumber spectrum. This was done by testing multiple values, and visually choosing a value that provides a good balance between smoothness and least impact on higher frequencies (e.g. Figure S4).

References

Cokelaer, T., & Hasch, J. (2017). 'spectrum': spectral analysis in python. *Journal of Open Source Software*, *2*(18), 348.

Dove, L. A., Thompson, A. F., Balwada, D., & Gray, A. R. (2021). Observational evidence

of ventilation hotspots in the southern ocean. *Journal of Geophysical Research: Oceans*, *126*(7), e2021JC017178.

Klymak, J. M., Crawford, W., Alford, M. H., MacKinnon, J. A., & Pinkel, R. (2015). Along-isopycnal variability of spice in the north pacific. *Journal of Geophysical Research: Oceans*, *120*(3), 2287–2307.

McDougall, T. J., & Krzysik, O. A. (2015). Spiciness. *Journal of Marine Research*, *73*(5), 141–152.

Prerau, M. J., Brown, R. E., Bianchi, M. T., Ellenbogen, J. M., & Purdon, P. L. (2017). Sleep neurophysiological dynamics through the lens of multitaper spectral analysis. *Physiology*, *32*(1), 60–92.

Stommel, H. (1962). On the cause of the temperature-salinity curve in the ocean. *Proceedings of the National Academy of Sciences of the United States of America*, *48*(5), 764.

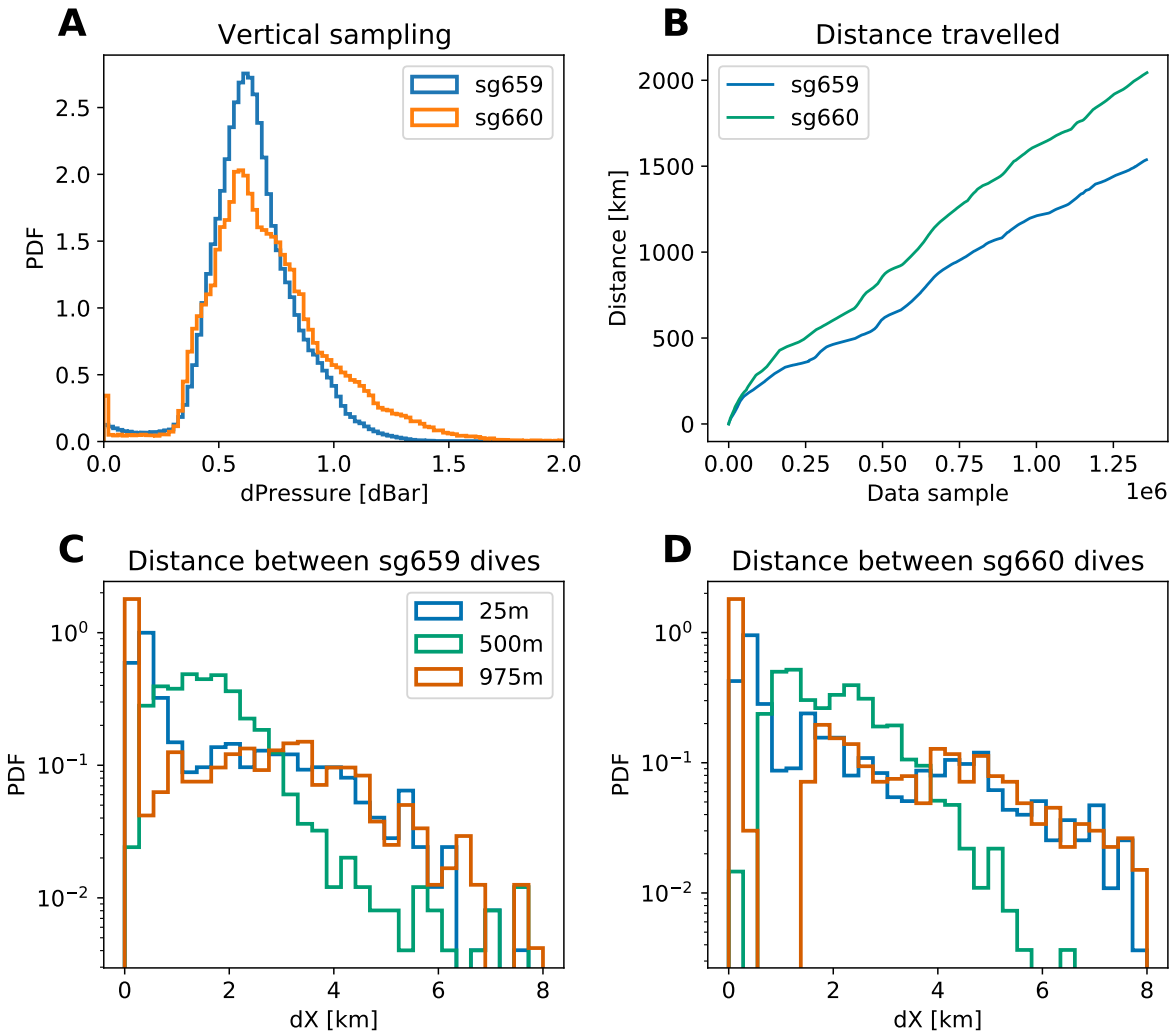

Figure S1. Sampling properties of the two gliders as a function of pressure (a) and distance between dives at different depths (c and d). (b) shows the cumulative distance traveled by the glider as a function of sample, where each point measurement is a sample.

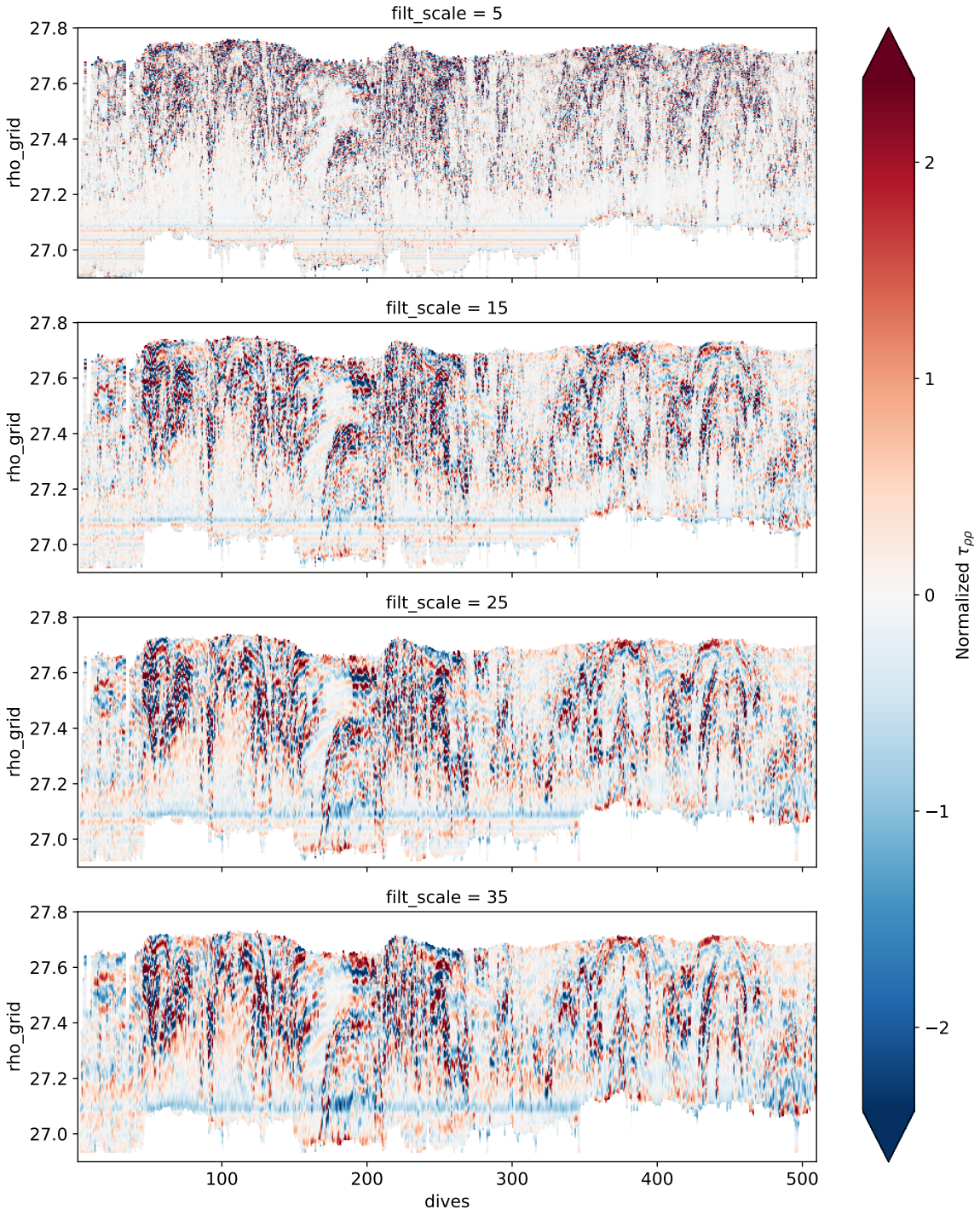

Figure S2. Normalized diapycnal spice curvature (DSC, $\tau_{\rho\rho}$/ divided by its standard deviation) for different filter scale choices, indicating the sensitivity of layering plots to filtering scale.

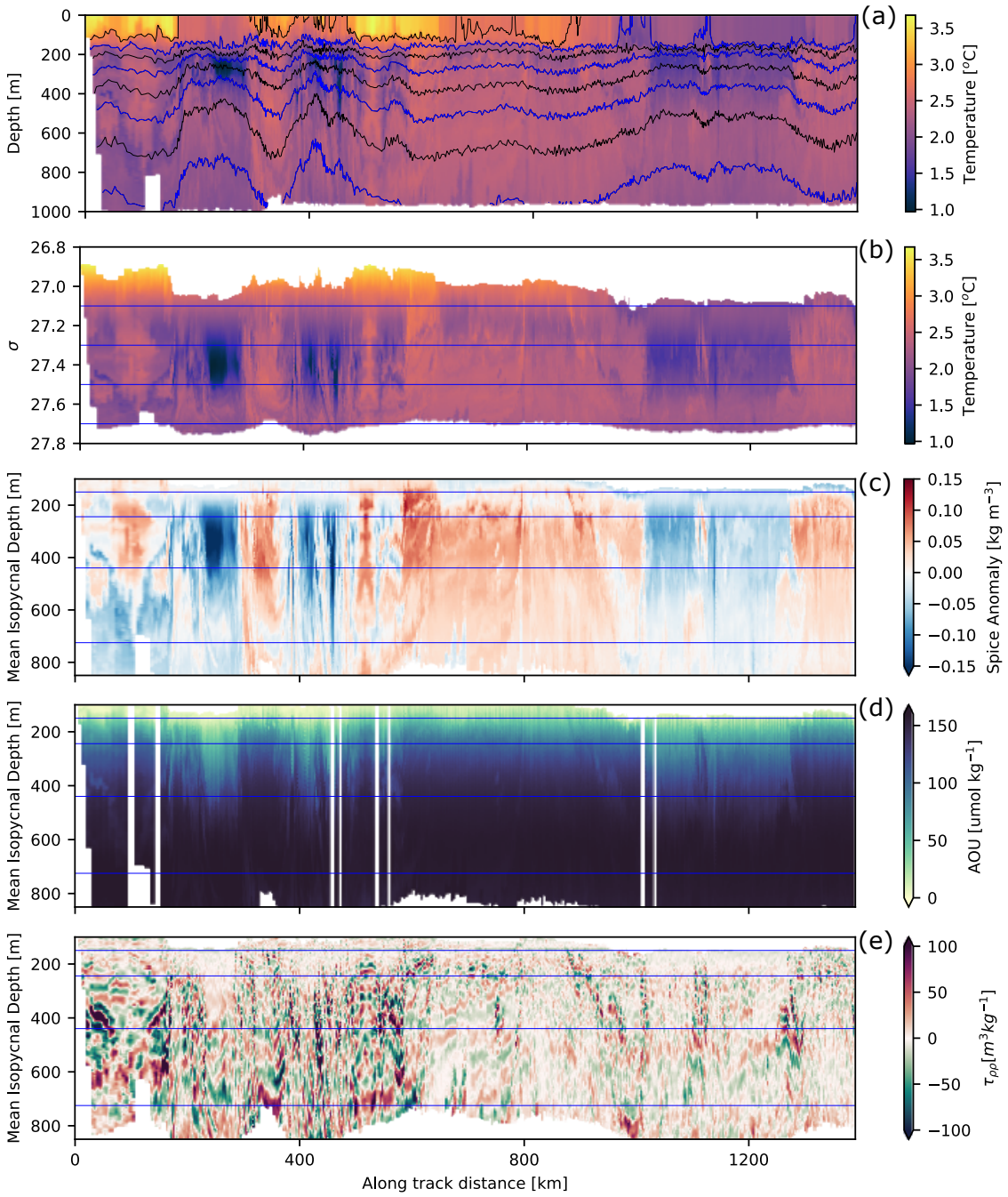

Figure S3. Sections from glider SG659 plotted as a function of along track distance. (a) Conservative temperature and isopycnals (potential density, black and blue contours with levels spaced by 0.1 kg m $^{-3}$) as a function of depth. (b) Conservative temperature as a function of isopycnal potential density. (c) Spice anomaly as a function of mean isopycnal depth. (d) Apparent oxygen utilization (AOU) as a function of mean isopycnal depth. (e) Diapycnal spice curvature, a metric to visually show layering, as a function of mean isopycnal depth. Horizontal blue lines in panels (b), (c), (d), and (e) indicate the mean depth of the 27.1, 27.3, 27.5, and 27.7 potential density surfaces, which are shown as blue contour lines in (a). Note that the x-axis in these plots is along track distance, which is different from the yearday time shown in Figure 1 in the main text.

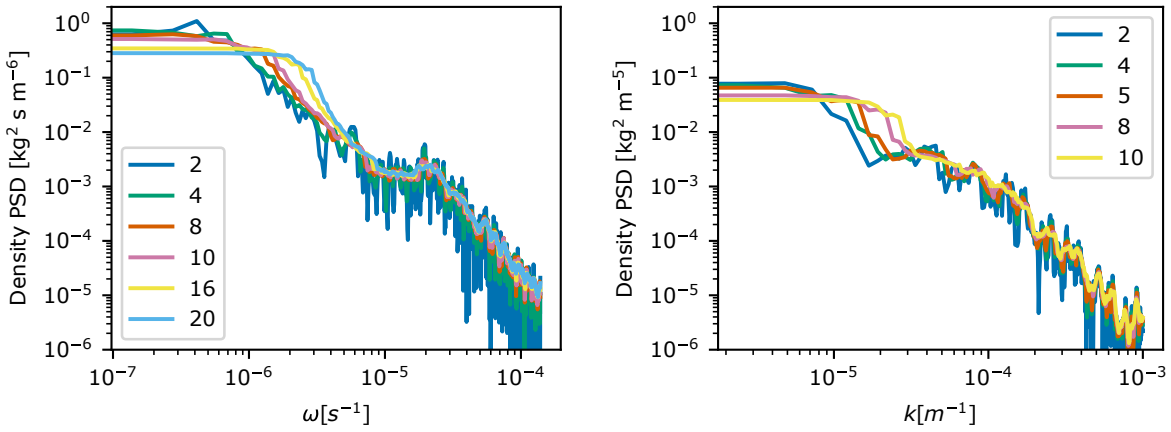

Figure S4. Sensitivity of the power spectral estimation to the choice of half-bandwidth parameter (N_w) for the frequency (left panel) and wavenumber (right panel) spectra. Nw is in the number of grid points, which is 1 hour for time and 500 m for space.

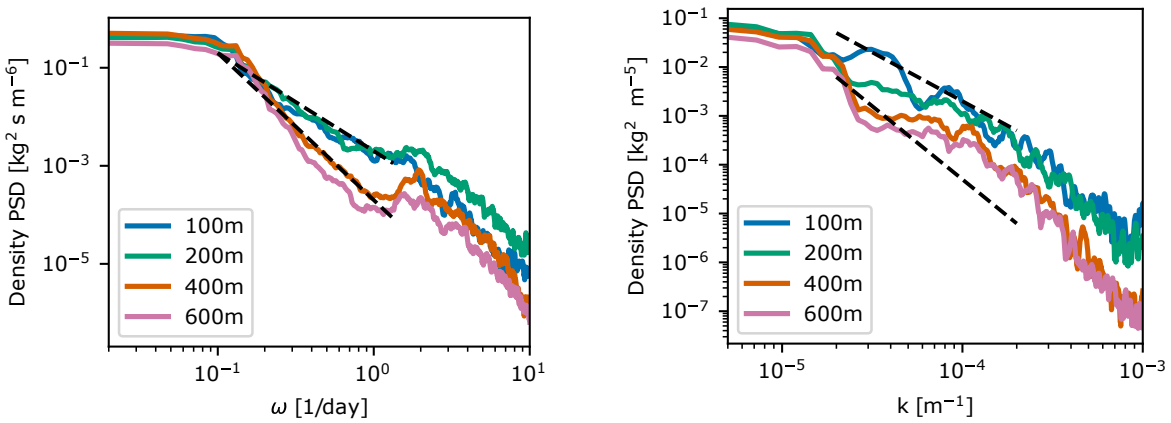

Figure S5. Line plots showing the frequency (left panel) and wavenumber (right panel) power spectra of density at different depths. This figure is complementary to Figure 3 in the main text, which shows the same spectra as 2D contour plot. The dashed black lines correspond to power law slopes of -2 and -3 respectively, and are plotted over the range of scales that the fitting was done to obtain the slope estimates in Figure 3.

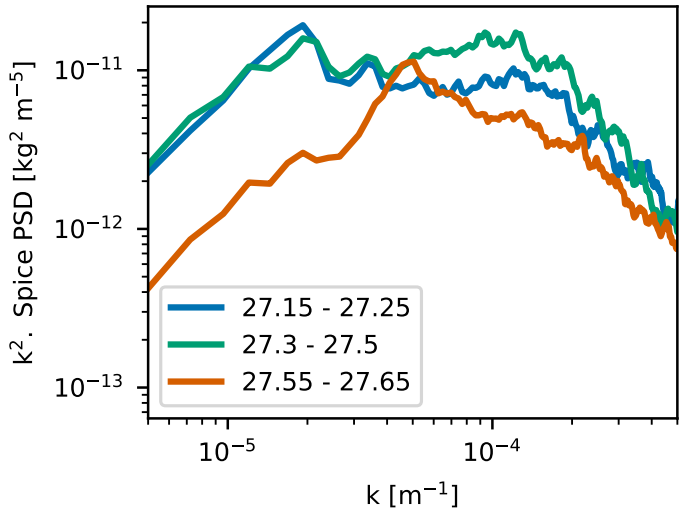

Figure S6. Along isopycnal spice power spectrum averaged over different density ranges plotted in a whitened (multiplied by k^2) form to allow an easy comparison of the slope relative to a k^{-2} power law. The estimation for this figure was done using only the data from the relatively straight glider section in the middle of the sampling period.

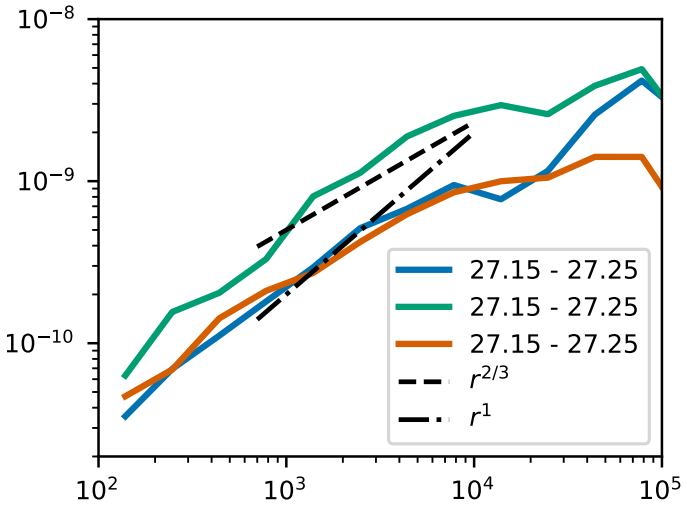

Figure S7. Along isopycnal spice SF2 averaged over different density ranges, plotted as line plots for easier visual detection of slopes and saturation scales. The dashed black lines correspond to power law slopes of 2/3 and 1 respectively, and are plotted over the range of scales that the fitting was done to obtain the slope estimates in Figure 6b.

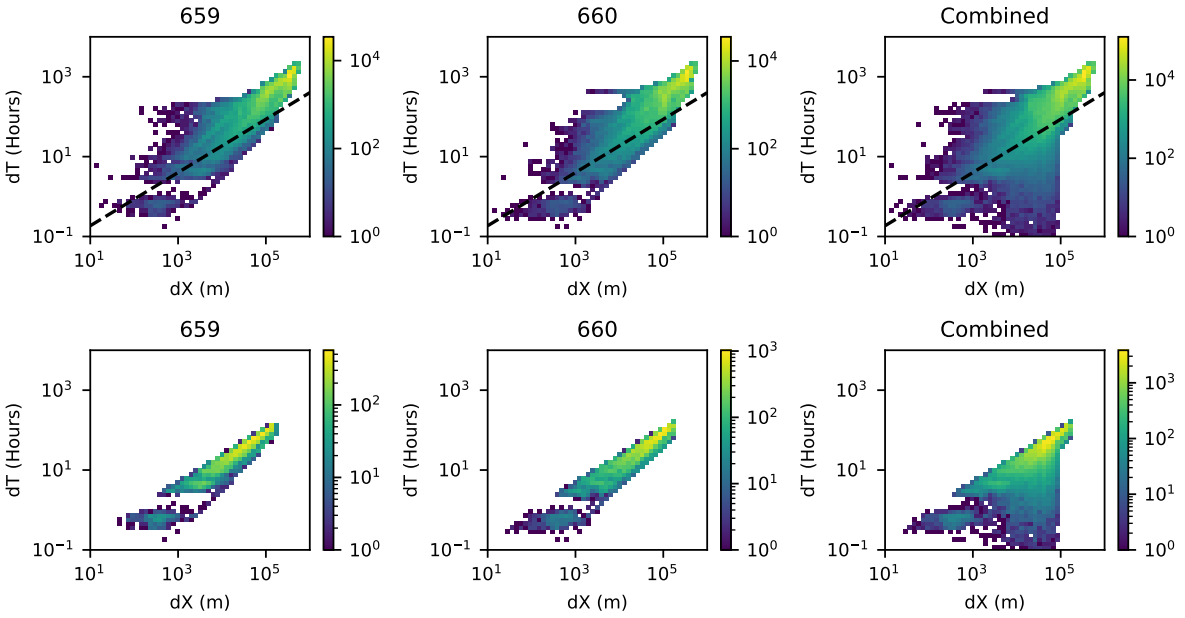

Figure S8. Distribution of sample pairs as a function for SG659 alone (left), SG660 alone (middle), and both gliders together (right). Top panels shows distribution of all possible pairs, and bottom panel shows distribution of pairs that were selected for computing binned statistics. The extra lobe of samples at short times and large scales only appears when both gliders are considered together, corresponding to time when the two gliders were far apart geographically. Dashed black line in top panels corresponds to the cut-off time scale, which is a function of spatial scale. Pairs that come from samples that are farther away in time than this cut-off time scale were not considered when computing binned statistics.